EFFECTS OF GAP WIDTH ON EUV TRANSMISSION THROUGH SUB-MICRON PERIOD, FREE-STANDING, TRANSMISSION GRATINGS

THESIS
Submitted to the College of Arts and Science of
West Virginia University
In Partial Fulfillment of the Requirements for
The Degree of Master of Science

By
Matthew M. Balkey
January, 1998

ABSTRACT

Sub-micron period, free-standing, transmission gratings have been designed as extreme ultraviolet light (EUV) filters for neutral atom imaging of the earth's magnetosphere. The effects of gap width on the transmission coefficient of EUV light are reported. Results from computations and an analytical waveguide model are shown to be consistent with the experimentally measured transmission coefficients. These results show that thin gratings with narrow gaps and thick gratings with large gap widths are equally effective at eliminating 121.6-nm radiation. The thin gratings with the narrow gaps have the advantage of better attenuation of shorter wavelength radiation (e.g., the 58.4-nm line of helium) than the thick gratings with the larger gaps. These findings have led to the development of thinner gratings with narrow gaps, rather than thick gratings for neutral atom imaging instruments.

TABLE OF CONTENTS

THEORETICAL AND COMPUTATIONAL INVESTIGATIONS

Our interest in sub-micron period, free-standing, transmission gratings arises from their potential use as extreme ultraviolet light (EUV) blocking filters in neutral atom imaging detectors.[1] An effective neutral atom imager requires the ratio of transmission coefficients for particles to 121.6-nm EUV to exceed 10^5.[1-3] Previous measurements of, and computational calculations for, 200-nm period gratings with 70-nm gaps and 130-nm bars[4-6] suggest that thick gratings (thickness > 700-nm) should achieve the needed rejection level. Construction of gratings with aspect ratios (thickness to gap width) greater than 10, is mechanically difficult. To predict the extreme ultraviolet light transmission of a grating before construction, an analytical parallel plate waveguide model has been developed and numerical calculations have been performed. The computations are consistent with the predictions of the analytical model and indicate that considerably thinner gratings with narrower gaps (≈ 40-nm) can achieve the required EUV rejection levels. As shown here, the narrower-gap gratings have the added advantage of more effectively eliminating shorter wavelengths such as the 58.4-nm helium line. Such background light rejection is critical for neutral atom imaging of the Earth's magnetosphere using existing detector designs.[1]

In the following section, the grating configuration is reviewed and the equations for transmission of radiation through two parallel, resistive, plates are presented to illustrate the role played by the gap in determining the overall transmission of TE and TM polarized electromagnetic radiation. The computational calculations for a complete grating structure are discussed in section II, the experimental apparatus is reviewed in section III, and the experimental measurements are presented in section IV.

I. GRATING STRUCTURE AND TRANSMISSION THROUGH PARALLEL PLATES

Our gratings were constructed at the Massachusetts Institute of Technology's NanoStructures Laboratory using techniques developed for the Advanced X-ray Astrophysics Facility (AXAF) satellite.[7-9] The grating period is established upon a photoresist surface by an interference pattern arising from the mixing of two beams of a 351.1-nm argon-ion laser. The resulting mask is processed further, allowing the deposition of gold between the bars of the mask. The remaining photoresist is then etched away, leaving a 200-nm period grating resting on a layer of plating base material. Because the grating is too weak to support itself, two support gratings fabricated by ultraviolet lithography are superimposed atop of the 200-nm period grating, as depicted in Figure 1, and the plating base is etched away. The transparency of the support structure is roughly 50% and the typical grating thickness is 500 nm.

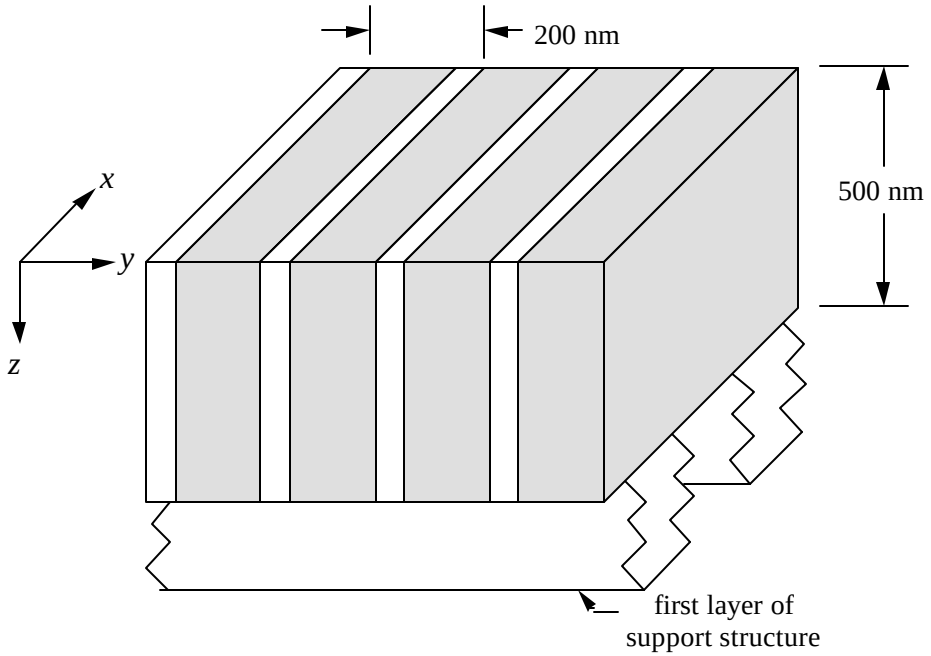

Figure 1. The schematic depicts a 500-nm thick free- standing gold grating with a 200-nm period. The shaded region is solid gold separated by vacuum. The support structure maintains the structural integrity of the grating.

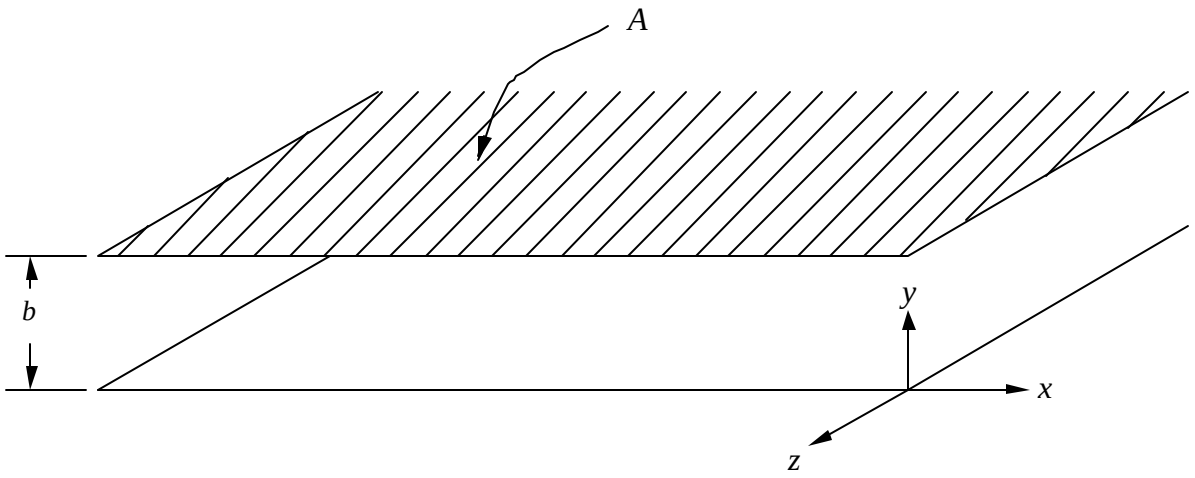

Figure 2. The coordinate system used for the parallel plate waveguide model. Two parallel plates are separated by a gap *b*. *A* is the surface area of each of the parallel plates. Wave propagation is in the *z* direction.

A parallel plate waveguide, illustrated in Figure 2, can be used as a simple model for these gratings. Conductive boundaries are located at $y = 0$ and $y = b$ and there are no boundaries in the *x*-direction. Wave propagation is along *z*. A semi-infinite waveguide model is physically justified, as the primary wavelength of interest, 121.6-nm, is small compared to the thickness, measured along *z*, and the length, measured along *x*, of the gratings. Interference and diffractive effects, which can be significant,[10] are ignored under these assumptions.

Unpolarized light incident on the grating can be separated into the TE and the TM polarizations.[11] The TE component obeys the dispersion relation

$$\left(\frac{w}{c}\right)^2 = k^2 + \left(\frac{np}{b}\right)^2 \tag{1}$$

in the case of a perfect conductor. The integer *n* denotes the Fourier mode of the TE component.[11] For $w < w_c = pc/b$, i.e., $l > l_c = 2b$, $\vec{k}$ is purely imaginary. Below this frequency cutoff, the wavelength is too large to fit between the walls of the waveguide. Above cutoff, $w > w_c$, the wave propagates without losses through a waveguide with perfectly conducting walls. The finite conductivity of any real material causes dissipation of the wave energy due to ohmic losses to the metal.

The wave fields that satisfy boundary conditions for the TE polarization are

$$
\begin{aligned}
E_x &= E_0 \sin\left(\frac{npy}{b}\right) e^{i(kz-wt)}, \\
B_y &= \frac{kc}{w} E_0 \sin\left(\frac{npy}{b}\right) e^{i(kz-wt)}, \\
B_z &= \frac{ic}{w}\frac{np}{b} E_0 \cos\left(\frac{npy}{b}\right) e^{i(kz-wt)}.
\end{aligned}
\tag{2}
$$

The Ohmic power loss per unit area can be calculated from[11]

$$
\frac{dP_{loss}}{dA} = -\frac{1}{2sd}\left|k_{eff}\right|^2, \tag{3}
$$

where d is the frequency dependent skin depth, s is the conductivity of the metal walls, $\vec{k}_{eff} = c/4p\left(\hat{n}\times\vec{H}_{||}\right)$, and $dA = dxdz$. Substituting into equation (3) gives the relation

$$
\frac{dP_{loss}}{dxdz} = -\frac{wd}{8p}\left|\frac{c}{w}\frac{np}{b}E_0\right|^2 . \tag{4}
$$

From the wave fields in equation (2), the component of the time-averaged Poynting vector in the z direction is

$$
\left\langle S_z \right\rangle = \frac{c}{8p}\frac{kc}{w}\left|E_0\right|^2 \sin^2\left(\frac{npy}{b}\right) . \tag{5}
$$

Integrating the Poynting vector over dy with the limits of integration at y=0 and y=b, gives the power incident per unit length on the grating

$$
\frac{dP_0}{dx} = \frac{c}{8p}\frac{kc}{w}\left|E_0\right|^2\frac{b}{2} . \tag{6}
$$

The power transmitted through the waveguide, the Poynting vector, decays exponentially as[11]

$$
P(z) = P_0 e^{-2bz} . \tag{7}
$$

Differentiating equation (7) to obtain the power loss per unit area yields,

$$\frac{dP}{dxdz} = \frac{dP_0}{dx}(-2\beta)e^{-2\beta z} \quad . \tag{8}$$

Assuming that β is small, equation (8) becomes

$$\frac{dP}{dxdz} = \frac{dP_0}{dx}(-2\beta). \tag{9}$$

Combining equations (4), (6), and (9) to solve for the attenuation coefficient β: yields,

$$2\beta_{TE} = \frac{d2|n\pi|^2}{k\beta^3}, \tag{10}$$

for the TE polarization. Note that the exponential dependence is proportional to $-z/\beta^3$. The power transmitted through the waveguide in the TE polarization can be reduced by decreasing the gap width, *b*, or by increasing the thickness of the grating, measured along *z*. Due to the β^{-3} term, a small change in the gap width has a significantly greater effect than a comparable change in the thickness of the grating.

Below cutoff, $\omega < \omega_c$, the wavevector, $\vec{k}$, is purely imaginary and the fields inside the conductor decay as e^{-kz} for perfectly conducting walls. The power transmitted through a real waveguide below cutoff decays due to the evanescent character of the wave and the resistive losses to the walls. To calculate these resistive losses, the evanescent fields inside the conductor are used. The electric field is calculated from[11]

$$\vec{E}_c = \sqrt{\frac{\mu_c \omega}{8\pi\sigma}}(1-i)\left(\hat{n}\times\vec{H}_{||}\right)e^{-y/d}e^{iy/d} \quad . \tag{11}$$

Using the fields for TE polarized radiation, equation (2), with $\vec{k} = i\vec{k}_I$, the real part of the electric field in the conductor is:

$$Re\left(\vec{E}_c\right) = \hat{x}\sqrt{\frac{\mu_c \omega}{8\pi\sigma}}\frac{n\pi}{b}\frac{c}{\omega}E_0 e^{-k_I z}\cos(\omega t). \tag{12}$$

Combining equation (12) with the real part of the magnetic field to calculate the real part of the Poynting vector directed into the conductor at *y* = 0 yields

$$\frac{dP_{loss}}{dxdz} = Re\left(S_y\right) = -\sqrt{\frac{m_c w}{8ps}}\frac{c}{4p}\frac{(np)^2}{b^2}\frac{c^2}{w^2}\left|E_0\right|^2 e^{-2k_I z}\cos(wt)\sin(wt)\ , \tag{13}$$

which is the power per unit area directed into the conducting wall, i.e., the Ohmic losses.

The real part of the Poynting vector along z can be found using the fields in equation (2) and allowing for an imaginary component of the wave vector

$$Re\left(S_z\right) = \frac{c}{4p}\left|E_0\right|^2 \sin^2\left(\frac{npy}{b}\right)\frac{k_I c}{w}e^{-2k_I z}\cos(wt)\sin(wt). \tag{14}$$

Integrating equation (15) over y with limits of integration of $y=0$ and $y=b$ gives the power per unit length incident on the grating

$$\frac{dP_0}{dx} = \frac{c}{4p}\frac{k_I c}{w}\left|E_0\right|^2 \frac{b}{2}\cos(wt)\sin(wt)e^{-2k_I z}\ . \tag{15}$$

As done in the case above cutoff, equations (9), (13), and (15) can be combined, assuming that $m_c = 1$ in the conductor, yielding the attenuation coefficient due to resistive losses below cutoff,

$$2b_{TE} = \frac{d2\left|np\right|^2}{k_I b^3}\ . \tag{16}$$

Except that k_I replaces k., this result is identical to equation (10) for the resistive losses above cutoff. The combination of the resistive losses to the metal walls and the evanescent character of the wave below cutoff leads to negligibly small transmitted power for radiation in the TE polarization below cutoff. Below cutoff, the power transmitted per unit length goes as:

$$\frac{dP}{dx} \propto e^{-(2k_I + 2b_{TE})z}\ . \tag{17}$$

For a parallel plate waveguide, the TM polarization is the same as the free space TEM polarization. The TEM polarization obeys the free space dispersion relation,

$$\frac{w}{c} = k\ , \tag{18}$$

and there are no cutoff conditions imposed by the boundaries. The only attenuation of TEM radiation is caused by resistive losses to the conductor. The transmitted power will have the same form as equation (2).[11] Starting with the wave fields for the TEM component,

$$\begin{aligned} E_y &= E_0 e^{i(kz - wt)} \\ B_x &= -E_0 e^{i(kz - wt)} \end{aligned}, \tag{19}$$

and following the same procedure used above to find the attenuation of the TE component, the attenuation coefficient for the TEM component is

$$2b_{TEM} = d\frac{w}{2cb}. \tag{20}$$

The exponential decay constant for the TEM component is proportional to $-z/b$. The resistive losses can be increased by decreasing the gap width, *b*, or by increasing the thickness of the grating. Increasing the thickness of the grating simply provides more surface area for resistive losses, but the gap effect is due to the structure of the wave fields responsible for the surface currents in the waveguide walls. To reduce the TEM transmission, a smaller gap is just as effective as a thicker grating. Note that the gap effect is exponential, not a simple linear decrease in transmission that might be expected for a waveguide with a narrower opening.

Using gratings that have approximately 10% transmission for neutral atoms, a transmission coefficient of 10^{-6} for 121.6-nm radiation is required for neutral atom imaging of the earth's magnetosphere[1]. A polarizer eliminates half the incident power of unpolarized light, the TE component, by operating below cutoff. This analytical waveguide model suggests that to achieve an EUV transmission coefficient of 10^{-6}, the resistive dissipation of the TEM component can be increased by using gratings with narrower gaps or by making the gratings thicker.

The background radiation reflected from the earth's geocorona includes wavelengths shorter than 121.6-nm. The intensity at these shorter wavelengths is less than the intensity of the 121.6-nm light,[12] but can generate substantial background during measurements of neutral atoms. Although the TE components at these wavelengths, such as the 58.4-nm helium line, are above cutoff for a grating with a

60-nm gap, the resistive effects of the gold grating attenuate the transmitted intensity as $e^{-2d(np)^2 z/(kb^3)}$. Previous calculations showed that, above cutoff, the transmitted power is dominated by the TE component.[4] Therefore, this simple waveguide model also suggests that gratings with a smaller gap will be much more effective at reducing the transmitted intensity of shorter wavelengths than thicker gratings.

II. COMPUTATIONAL SIMULATION OF GRATING PERFORMANCE

Computational simulations of grating transmission were performed using the three-dimensional, full-wave, vector code Gsolver.[13] With this code, it is possible to model a grating that has a periodicity in the *y* direction, is infinite in the *x* direction, and has a finite thickness along *z*. The boundary conditions at all of the surfaces, the finite conductivity of gold, and reflections from the front surface of the grating are included in the computational results. Adjustable parameters include the period, the thickness of the grating, the gap between the gold bars, the angle of polarization of the incident radiation, and the wavelength of the incident radiation. The user supplied the index of refraction of gold as a function of wavelength.[14] For neutral-atom imaging of the Earth's magnetosphere, the experimental configuration of interest is unpolarized 121.6-nm light incident on a gold grating with a period of 200 nm.[1] Transmission coefficients predicted by the waveguide model and computational calculations, for various values of the gap and thickness of the grating are compared. Transmission at shorter wavelengths, primarily 58.4-nm, is also investigated.

Figure 3 shows computational results for 121.6-nm light incident on a gold grating with a 200-nm period. The transmission coefficient of the TE component exhibits the same dependence on *b* as predicted by the analytical model. As seen previously,[4] the TE mode dominates the overall transmission through the grating above cutoff. The waveguide model predicts a TE transmission coefficient of $5.97 \times 10^6 b|E_0|^2 e^{-3.82 \times 10^6 \text{ nm}^3/b^3}$ and a TEM transmission coefficient of

$5.97 \times 10^6 b|E_0|^2 e^{-516 \text{ nm}/b}$ above cutoff. Assuming that equal amplitudes of TE and TEM radiation enter the grating, the waveguide model predicts that the TEM mode should dominate the overall transmission for gap widths between 60-nm and 121.6-nm. For gaps larger than 121.6-nm the TE component should dominate the transmission. The discrepancy between the waveguide model and the computational results occurs because gold is a poor conductor at the frequency of interest. Computations performed using indices of refraction for a good conductor yielded results that agree with the waveguide model in both magnitude and scaling with the gap width.

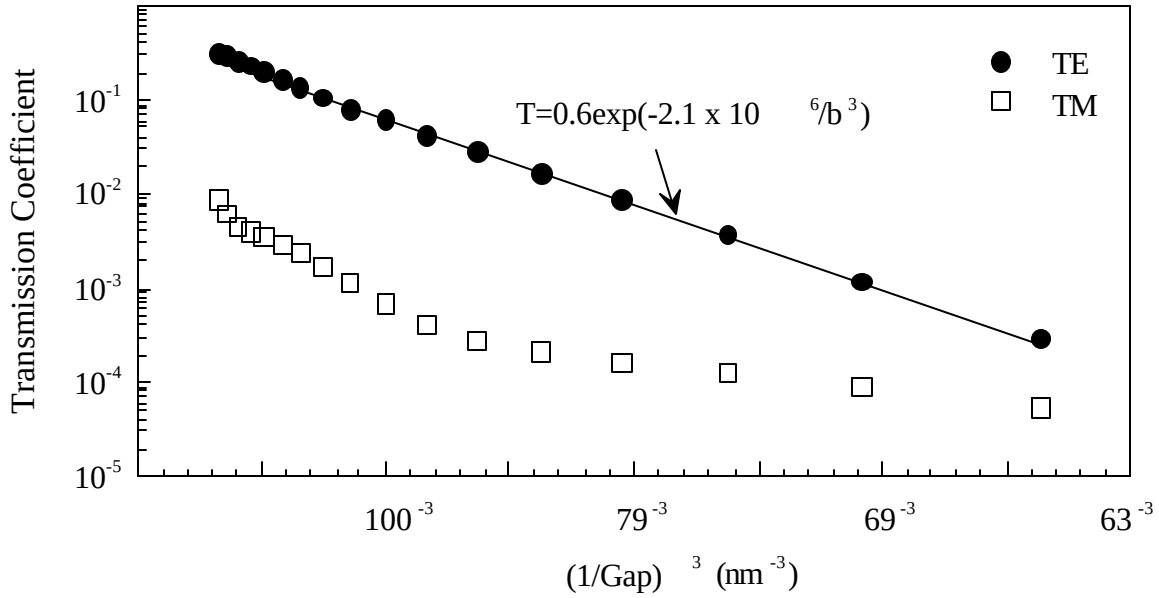

Figure 3. Computational results for TE and TEM transmission above cutoff as a function of gap width for a 500-nm thick grating with a period of 200 nm. The TE component dominates the transmission.

Figure 4 shows the effects of gap width on transmission below the TE cutoff. As the waveguide model suggests, the computationally calculated TEM component dominates the overall transmission below cutoff but is not well fit with a single $e^{-z/b}$ type relationship. The computational results suggest that the physics of the TEM transmission below cutoff is more complicated than the physics of the simple waveguide model. However, the TEM transmission coefficient does decay exponentially as a function of 1/*b* - consistent with the predictions of the waveguide model below cutoff.

In order to obtain the required rejection level for 121.6-nm radiation, thick gratings or gratings with small gap widths can be used. Because of limitations in the fabrication process, it is difficult to produce gratings that are both very thick and have narrow gaps. Figure 5 shows the total transmission versus thickness for several gaps and a 200-nm period. For gratings with gaps less than $l/2$ (below the cutoff for TE waves), the transmission is dominated by the TEM component as shown in Figure 4. According to Figure 5, for a grating with a 40-nm gap, the computations indicate that the grating must be 450-nm thick to achieve 10^{-6} transmission for 121.6-nm radiation. For the same performance from a grating with a 60-nm gap, the grating

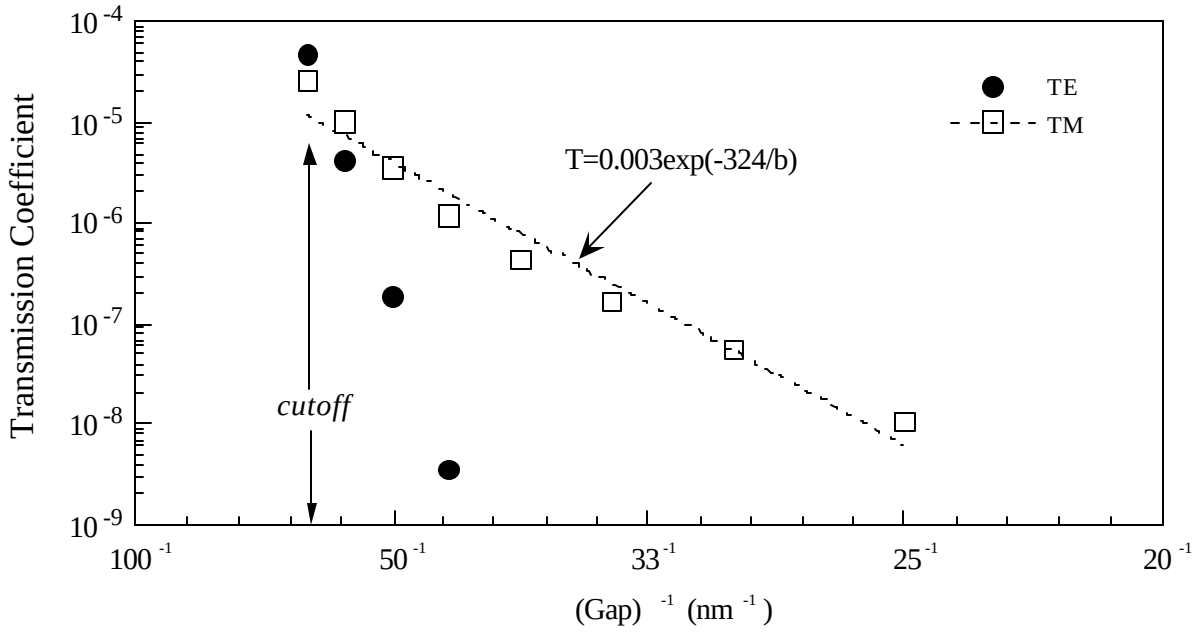

Figure 4. Computational results TE and TEM transmission below cutoff as a function of gap width for a 500-nm thick gold grating with a 200-nm period. The computational results are not well fit by a single $e^{-1/b}$ type function.

must be 700-nm thick. The ratio of thickness to gap width is 11.3 for the 450-nm thick grating and is 11.6 for the 700-nm thick grating. Therefore, these two gratings are equally difficult to make and would give the same attenuation of 121.6-nm light. However, the thinner grating with the narrower gap has the additional advantage of better attenuation of shorter wavelength radiation, e.g., the computed

transmission coefficient for the 58.4-nm helium line is 1.9 x 10^{-4} through the thinner grating and 4.4 x 10^{-3} through the thicker grating: a result of the $1/b^3$ dependence in the exponent in equation (11).

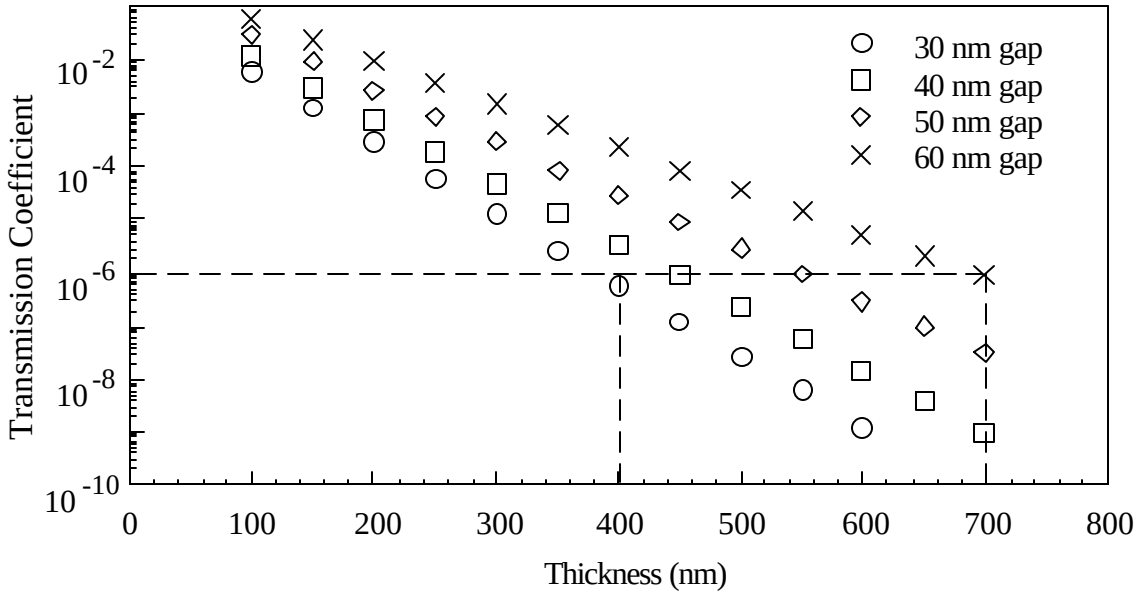

Figure 5. Computational results for total transmission through 200-nm period grating as a function of grating thickness for different gap widths. The dashed lines mark the grating thickness required for a transmission coefficient of 10^{-6} if *b=30*-nm or *b=60*-nm.

LIGHT SOURCE AND EXPERIMENTAL MEASUREMENTS

A set of gratings received from Massachusetts Institute of Technology was tested in a monochromatic EUV test facility built at West Virginia University.[15] Testing these gratings quickly, accurately, and consistently, requires an intense, monochromatic, extreme ultraviolet light source. There are two standard techniques for generating monochromatic 121.6-nm light for such testing purposes: a gas discharge coupled to a vacuum ultraviolet, grazing-incidence-monochromator;[16] or a synchrotron light source.[5-6] Both of these techniques require an extensive vacuum system and costly ancillary equipment. In addition, the grazing-incidence-monochromator approach results in insufficient signal

through a grating with a transmission coefficient of 10^{-6}. Because the light source does not have to be highly monochromatic (a source with a FWHM of a few nanometers is sufficient) it is possible to trade light source monochromaticity for ease of operation from compact light source.

III. LIGHT SOURCE DESCRIPTION

The essential components of the light source are a 30-W Hamamatsu deuterium lamp with primary emission in the range 120 to 200-nm, two 10-nm FWHM bandpass filters with a central wavelength of 121.6-nm, an ultraviolet-to-visible conversion phosphor, and a high sensitivity photomultiplier-tube detector as depicted in Figure 6. The convolution of the deuterium lamp spectrum (data supplied by manufacturer) and the narrow bandpass filter transmission characteristics (supplied by manufacturer) in the extreme ultraviolet is shown in Figure 7. The deuterium lamp was constructed with a magnesium fluoride window to permit emission of 121.6-nm light. As shown in Figure 7, the filtered lamp spectrum has a full-width-half-maximum of roughly 2.5-nm, centered at 121.6-nm. The lamp also emits strongly in the visible and a second bandpass filter was required to improve the ratio of ultraviolet to visible light to 10^5.

After passing through the bandpass filter, the EUV passes through a shutter mechanism and illuminates a sliding mount that holds one free-standing grating and a calibrated neutral density filter (transmission coefficient = 1.4×10^{-6} at 121.6-nm). Behind the sliding mount is a glass blank coated with approximately 1 mg/cm^2 of phosphorescent sodium salycilate. At that thickness, the sodium salycilate phosphor converts 120-nm ultraviolet light to visible 420-nm light with a quantum efficiency of approximately 80%.[17] Visible inspection of the phosphor-coated blank indicates that it is uniformly illuminated by the light source. Behind the glass blank is a Hamamatsu R6905 photomultiplier-tube detector with a gain of approximately 2×10^7 when biased with 1300 Volts. The peak of the photomultiplier-tube spectral response is centered at 420-nm. Since the photomultiplier-tube is a sealed unit, there is no need for a vacuum system for the photon detection system.

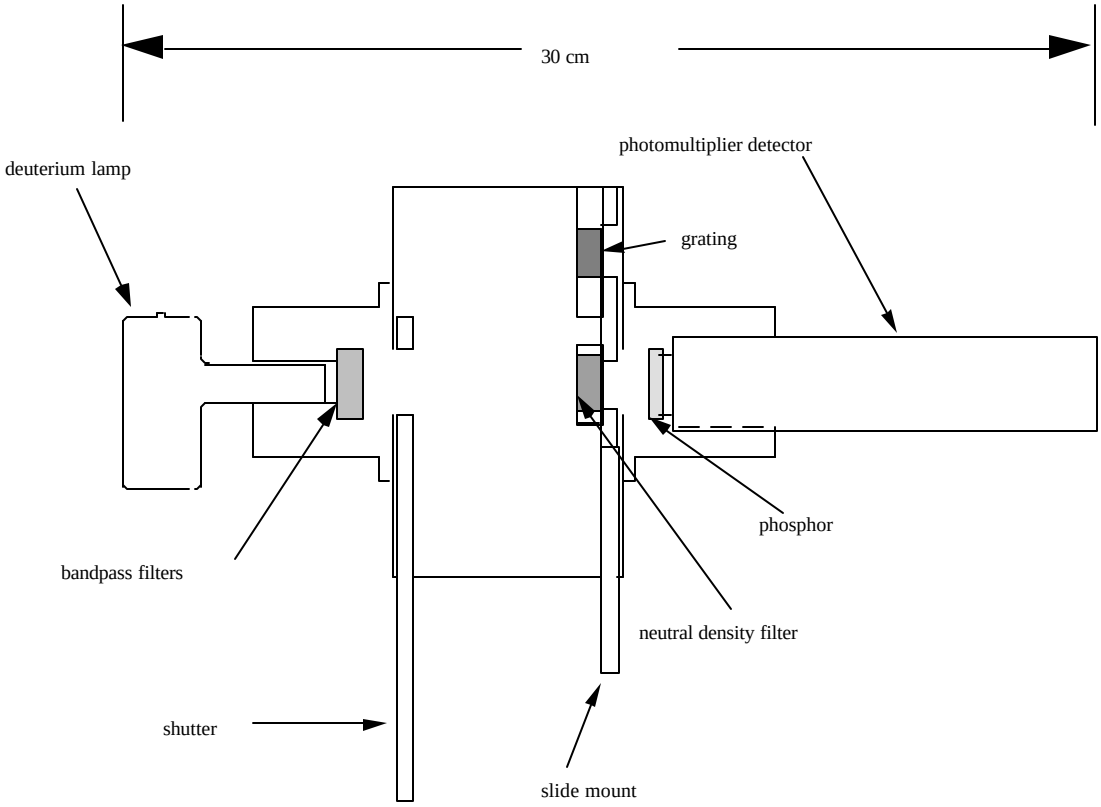

Figure 6. The compact 121.6-nm light source. The grating and filter can be conveniently interchanged using the slide mount.

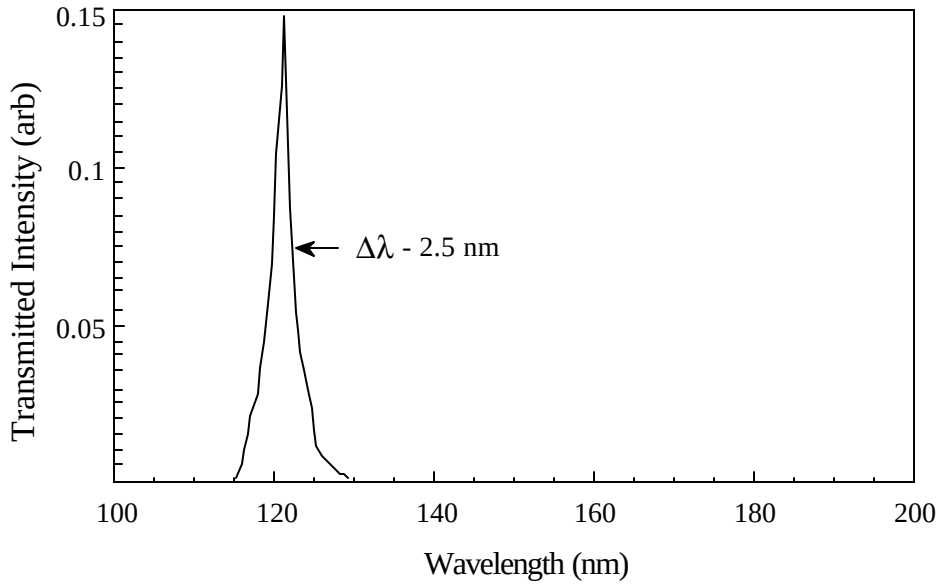

Figure 7. Calculated convolution of the measured deuterium lamp spectrum with the measured transmission characteristics of the narrow bandpass filter in the extreme ultraviolet. Hamamatsu supplied the lamp spectrum and Acton Research provided the filter specifications.

The entire apparatus is enclosed in aluminum housing through which a continuous purge of 99.99% helium gas flows. Helium has no absorption lines near 121.6-nm. Operation in a helium atmosphere greatly reduces the absorption of extreme ultraviolet light by water vapor, oxygen, and nitrogen molecules; thereby eliminating the need to place the filters and gratings in a vacuum system. For cleanliness purposes, the aluminum enclosure is housed in a sealed glove box. The glove box helps to reduce contamination of the free-standing gratings by dust and water vapor.

Considerable care has been taken to eliminate background light in the apparatus. The sliding mount and shutter mechanisms include a sliding o-ring slide for blocking light from going around the shutter and test objects. The bandpass filters, sodium salycilate phosphor, and photomultiplier are also mounted in the apparatus with o-ring seals. The measured background light due to external sources and from light leaking around the grating or neutral density filter mounts contributes less than 1% to the transmission measurements reported in the following section. If reduced signals levels are acceptable, the light source can be operated without the helium purge. Signal levels are reduced by more than an order of magnitu previously, the visible contributio use the typical grating transmissi e ultraviolet (a skin depth effect), ents is roughly 1%.

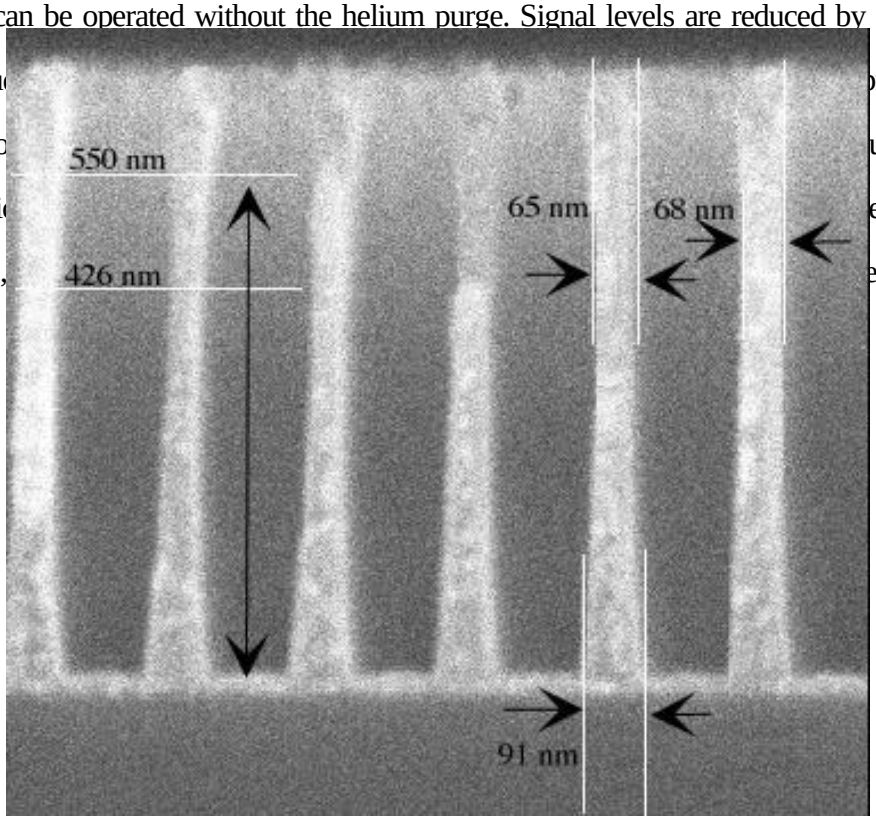

Figure 8. SEM photograph of the etched channel in the photoresist material before it is filled with gold. The thickness of the grating is approximately 550 nm. Note that the gap width ranges from 91-nm at the top and bottom to approximately 55-nm in the center.

For spatially localized measurements of the transmission coefficient for 121.6-nm light through the grating, a collimator can be inserted into the shutter aperture and can be scanned across the grating surface. The collimator illuminates a 2-mm diameter region on the grating or the reference neutral density filter.

IV. TRANSMISSION MEASUREMENTS

Before the etched lines in the photoresist material are filled with gold, samples are cleaved and examined with scanning electron microscopy (SEM). A SEM image of a sample photoresist structure is shown in Figure 8 and demonstrates the non-parallel edges of the gaps. The gap profile shown in Figure 8 is representative of the entire set of gratings, but there are variances across each individual grating and between different gratings. On average, the set of gratings has a minimum gap of 40 nm at the mid-plane and widen out to 70 nm at the top and bottom. After filling the photoresist with gold, the photoresist is etched away leaving gratings that are approximately 550 nm thick.

EUV transmission measurements of five gratings range from 9.1×10^{-6} to 1.1×10^{-4}, as shown in Figure 9. Multiple values of the transmission coefficient for a given grating were measured using the collimator to sample small portions of the grating, rather than the entire incident area (1.70 cm x 1.03 cm). The variances in the collimated results are caused by small differences in the gap across the grating surface, pinholes caused by the contamination of dust during processing of the grating, and strain around

the edge of the grating created by the gluing of the grating to a holder. The error associated with each point, caused by background light, is smaller than the data point.

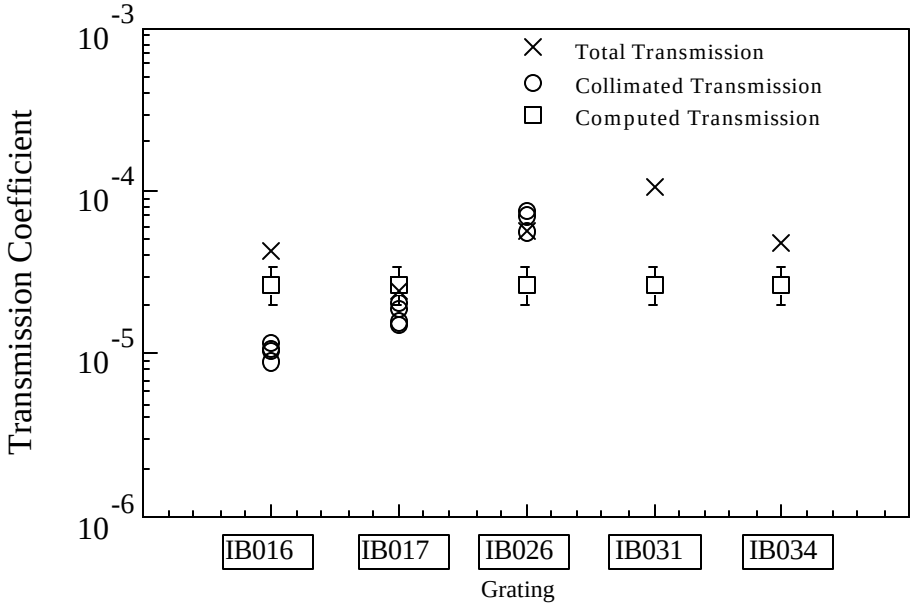

Figure 9. Open circles and X's denote experimental measurements of the 121.6-nm transmission through five gold gratings. The X's represent the transmission coefficient when the entire grating surface is illuminated. The open circles give the transmission coefficient for a small region (approximately 2-mm in diameter) of the grating. The computational predictions for a typical grating based on the measurements of the gap structure in the photoresist are indicated with open squares.

The agreement between the measurements and the computational results improve when the curvature of the gap is taken into account. This is accomplished using a tiered grating model with different gap widths at different heights as depicted in Figure 10. The SEM photo in Figure 8 was used as a template for the model. The error bars on the computational result were estimated by using the entire range of values for the index of refraction of gold at 121.6 nm available in the published literature.[14,18-19] The average computational results are within a factor of 3 of the experimental values for gratings IB016, IB017, and IB034. The two gratings with significantly larger transmission coefficients than predicted, gratings IB026 and IB031, had clear structural problems. Grating IB026 was damaged during processing, resulting in a large hole and other light leaks. SEM photos of IB031

show clumping of the gold bars. In some regions the bars are stuck together, resulting in doublewide bars and double wide slot gaps. According to the waveguide model, 121.6-nm light is above the TE cutoff for a doublewide slot gap. Thus the model qualitatively corroborates with the experimentally measured transmission for grating IB031.

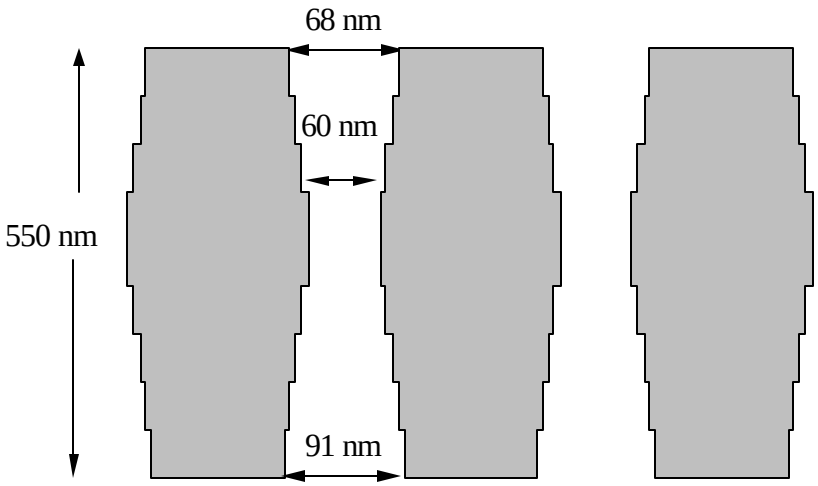

Figure 10. Tiered model of gap in the gold grating used in computational model. The gap between the bars narrows in the middle of the grating (the reverse of the photoresist image in Figure 8)

SUMMARY

An analytical model based on a parallel plate waveguide with resistive walls predicts that, below cutoff ($w < w_c = pc/b$), the TEM component will dominate the total EUV transmission through a 200-nm period grating. The model predicts that the resistive dissipation of the TEM component follows a $e^{-dwz/2cb}$ dependence on the gap width, b. Above cutoff, the transmission of the TEM component obeys the same exponential decay, but the TE component is resistively dissipated according to $e^{-2d(np)^2 z/kb^3}$.

The simulation of the grating performance using the Gsolver software confirmed that below cutoff, the TEM component dominates the transmission and generally obeys a $e^{-dw_z/2cb}$ type dependence on slot gap. Above cutoff, the computations indicate that the TE component dominates the transmission and scales as $e^{-2d(np)^2 z/kb^3}$. Experimental measurements of the transmission of 121.6-nm radiation through five 200-nm period gratings are in good agreement with computational predictions that include the detailed geometry of the gap structure. The typical EUV transmission coefficient of the gratings was 2 x 10^{-5}.

Based on the predictions of the waveguide model and the computational results, the MIT group has focused their efforts on developing 500-nm thick gratings with narrower gaps for neutral-atom imaging. The gratings with narrower gaps have less open area, so they reduce the neutral particle transmission as well as the EUV transmission. However, the particle transmission decreases linearly with the gap width while the EUV transmission falls off exponentially. In addition, the narrower slot gaps provide better rejection of shorter wavelength radiation above cutoff due to the $1/b^3$ effect in the exponential resistive loss term of equation (11). Computations for gratings currently under construction predict an EUV transmission coefficient at 121.6-nm of 2 x 10^{-6}, an order of magnitude better than the results reported here.

ACKNOWLEDGMENTS

I would like to thank Dr. Earl E. Scime for his guidance on this project, Dr. Mark Schattenburg, Joost van Beek and the MIT group for the gratings and SEM images, Dr. H. Arthur Weldon for his help in developing and understanding the waveguide model, Doug Mathess and Carl Weber for their expertise in the building of the apparatus, and the NIS-1 group at Los Alamos National Lab for the use of their facilities for grating testing.

REFERENCES

[1]E.E. Scime, H.O. Funsten, M.A. Gruntman, D.J. McComas, Opt. Eng. **33**, 357 (1994).

[2]M. A. Gruntman, "Submicron structures: promising filters in EUV - a review" in EUV, X-Ray, and Gamma-Ray Instrumentation for Astronomy, eds. O. H. Siegmund and R. E. Rothschild, Proc. SPIE **1549**, 385-394 (1991).

[3]D.J. McComas, H.O. Funsten, J. T. Gosling, K.R. Moore, E.E. Scime, and M. F. Thomsen, Opt. Eng. **33**, 335 (1994).

[4]E.E. Scime, E. H. Anderson, D. J. McComas, and M. L. Schattenburg, Applied Optics **34**, 648 (1995).

[5]M.A. Gruntman, Applied Optics **34**, 5732 (1995).

[6]M.A. Gruntman, Applied Optics **36**, 2203 (1997).

[7]M. L. Schattenburg, E. H. Anderson, and Henry I. Smith, "X-ray/VUV Transmission Gratings for Astrophysical and Laboratory Applications," Physica Scripta **41**, 13-20 (1990).

[8]M. L. Schattenburg, C. R. Canizares, D. Dewey, K. A. Flanagan, M. Hamnett, A. M. Levine, K. S. K. Lum, R. Manikkalingam, T. H. Markert, and H. I. Smith, "Transmission grating spectroscopy and the Advanced X-ray Astrophysics Facility (AXAF)," Opt. Eng. **30**, 1590-1600 (1991).

[9]J.M. Carter, D.B. Olster, M.L. Schattenburg, A. Yen, H.I. Smith, J. Vac. Sci. Technol. B **10**, 2909 (1992).

[10]H. Lochbihler, and P. Predehl, "Characterization of x-ray transmission gratings," Applied Optics. **31**, 964-971 (1992).

[11]J. D. Jackson, Classical Electrodynamics (John Wiley & Sons, New York, 1975), p. 334-384.

[12]R. R. Meier, Space Science Reviews. **58**, 1-185 (1991).

[13]available from the Grating Solver Development Company, Allen, TX 75013.

[14]D. E. Gray, ed., *American Institute of Physics Handbook* (McGraw-Hill, New York, 1972), pp. 6-118.

[15]Earl E. Scime and M. M. Balkey, “A Compact, Intense, Monochromatic, Atmospheric Pressure, Extreme Ultraviolet Light Source,” Rev. Sci. Instrum., submitted (1997).

[16]B.W. Smith, J.J. Bloch, D. Roussel-Dupre, Optical Engineering **29**, 592 (1990).

[17]J.A.R. Samson, *Techniques of Ultraviolet Spectroscopy* (John Wiley & Sons, New York 1967).

[18]Edward D. Palik, ed., *Handbook of Optical Constants of Solids* (Academic Press, New York, 1985), pp. 286-295.

[19]J.H. Weaver, C. Krafka, D.W. Lynch, D.W. and E.E. Koch, "Optical properties of metals. I. The transition metals," Physik Daten **18**, 1 (1981).